Resonant waveguide grating fabrication on planar and cylindrical substrates using a photosensitive TiO2 sol-gel approach

Maria Alejandra Usuga Higuita, Hugo Bruhier, Marion Hochedel, Thomas Kampfe, Francis Vocanson, Arnaud Valour, Damien Jamon, Michel Langlet, Nicolas Crespo-Monteiro, Yves Jourlin

Research Article | Vol. 11, No. 1 / 1 January 2021 / Optical Materials Express 12
Optical Materials EXPRESS

Resonant waveguide grating fabrication on planar and cylindrical substrates using a photosensitive TiO_2 sol-gel approach

MARIA ALEJANDRA USUGA HIGUITA,[1,2] HUGO BRUHIER,[1] MARION HOCHEDEL,[1] THOMAS KAMPFE,[1] FRANCIS VOCANSON,[1] ARNAUD VALOUR,[1] DAMIEN JAMON,[1] MICHEL LANGLET,[2] NICOLAS CRESPO-MONTEIRO,[1,3] AND YVES JOURLIN[1,4]

[1] *Université de Lyon, UJM-Saint Etienne, CNRS, Laboratoire Hubert Curien, UMR 5516, Saint-Etienne 42000, France*
[2] *Université de Grenoble Alpes, CNRS, Laboratoire des Matériaux et du Génie Physique (LMGP), UMR 5628, Grenoble 38000, France*
[3] *nicolas.crespo.monteiro@univ-st-etienne.fr*
[4] *yves.jourlin@univ-st-etienne.fr*

Abstract: A single-step sol-gel technological approach combining sol-gel layer development and UV lithography is demonstrated for the fabrication of resonant waveguide gratings (RWG) on planar and cylindrical substrates. The aim of this article is the demonstration of a resonant reflection in TE and TM polarization in the near-infrared region (NIR) in a planar and in cylindrical-based resonant waveguide gratings (RWG). In this work, we start with a planar corrugated waveguide structure excited by a planar wave and demonstrate this concept to a circularly symmetrical waveguide applied to the inside wall of an 8 mm diameter tube, excited by a cylindrical wave. For both configurations, the same TiO_2 sol-gel layer is used for the high index waveguide layer and for the grating printing thanks to the UV photosensitivity property of the sol-gel layers, avoiding any etching processes. The reflection spectrum was measured in the near-infrared range and compared to the modeling, showing the expected resonant behavior.

1. Introduction

Resonant waveguide gratings (RWG), also called Guided-Mode Resonance (GMR) gratings, have been discovered several decades ago [1,2] and are known for their possibility to very strongly reflect an incident wave for special configurations of the parameters of the optical setup like wavelength, polarization and incident angle [3]. An RWG consists of a high index waveguide and a periodic corrugation (grating) to couple the waveguide mode. Theoretically, 100% reflection efficiency can be achieved with a subwavelength period grating and a lossless waveguide layer. The grating and waveguide parameters are optimized numerically using RCWA (Rigorous Coupled Wave Analysis) [4] and C-method (Chandezon method) [5], according to the grating parameters. These methods allow optimizing the resonant grating, resulting in optimal parameters according to the application.

Applications are numerous and now widespread in optical components and industrial products [6], such as in the field of sensors [7,8], solar cells [8,9], filters [10,11], lighting [12], security [13] and polarizers [14] from UV to microwave frequencies [15,16].

There are many technologies to obtain RWGs. Techniques such as magnetron sputtering [17] CVD [18], ALD [19] and others permit to cover thin waveguide dielectric layers on various substrates. Concerning the grating fabrication, a well-known technique for the fabrication of subwavelength gratings is laser interference lithography [20] (LIL). It allows fabricating high coherent gratings on large substrates, and printing 1D and 2D gratings [21]. Remarkably, LIL can

#411560 https://doi.org/10.1364/OME.411560
Journal © 2021 Received 1 Oct 2020; revised 23 Nov 2020; accepted 23 Nov 2020; published 3 Dec 2020

Optical Materials EXPRESS

be applied to non-planar substrates, which is a big advantage over other grating manufacturing techniques such as nanoimprint lithography [11] and electron beam lithography [6]. Nevertheless after lithography process on sacrificial photoresist layers, etching process for grating printing on the dielectric layer remains an issue to be tackle.

Huang et al. [22] developed a technological process to manufacture planar resonant gratings in sol-gel layers using Nano-Imprint Lithography (NIL) for the grating fabrication. In this latter case, the NIL approach is very interesting and promising and remains compatible to sol-gel layers. But in the cylindrical structure, NIL approach is impossible, lithography approach is thus the unique possibility provided a UV photosensitive sol gel development and appropriate lithography set-up. Tonchev et al. [23] obtained a grating from organic photoresist printed on the outer wall of a glass cylinder using a single exposure with a radial phase mask designed for a wavelength of 442 nm. Later, Berthod et al., [24] printed a cylindrical grating in TiO_2 on the inner and on the outer wall of a tube by using a reversible phase mask, where the grating was made using a photosensitive TiO_2 sol-gel and a special optical bench. Koussi et al., [25] obtained the first cylindrical resonant grating. The waveguide layer was obtained using a TiO_2 sol-gel and the grating was realized with a positive photoresist (S1805). In addition, on this recent Ref. [25] the authors demonstrated only resonance for TE polarization with low efficiency.

In this article, we introduce a technological process to realize a resonant grating inside a cylindrical substrate using only a photosensitive TiO_2 sol-gel for the waveguide layer and the grating. The approach introduces the single-step photopatternable sol-gel layer method compatible to complex lithography set-up where both etching and NIL process can not be performed. Sol-gel layers can be deposited on large size and non-conventional substrates like cylinders [26], tubes [25] or plastics [27] using a dip-coating process. Moreover, this photosensitive sol-gel is also compatible with different lithography processes, as for example phase mask lithography [28] or colloidal lithography [29]. The authors introduce the design of the WRG, which they used to fabricate the resonant grating on cylindrical substrate. The optical responses demonstrating resonances of the device were then compared with planar resonant grating made under the same conditions.

2. Experimental methods

2.1. Simulation method

The structures were simulated with the commercial software MC GRATINGS using the Chandezon method (C-method). The two structures were simulated using the C-method (Chandezon method) with the module *ChandezonCol* of the commercial software *MC Grating*. The profiles of the experimental structures are rather sinusoidal, which explain our choice for this method compared to the RCWA (Rigorous Coupled Wave Analysis) method, which consists in expanding the dielectric permittivity function of the grating and the electromagnetic fields in the plane of the grating using Fourier harmonics and enforcing boundary conditions at the different interfaces. It is well adapted to binary or staircase-like profiles, whereas the C-method, which is based on solving the Maxwell's equations in curvilinear coordinates, allows the simulation of continuous grating profiles. The direct space is transformed in function of the grating profile to simplify the boundary conditions at the interfaces. The method performs the Rayleigh expansion of the field in the new curvilinear coordinates system and thus resolves the wave equation. An "extended" method was used, which allows us to have in the same structure different shapes for each interface: the first interface, the surface of the grating, is sinusoidal and the other are plane surfaces. In each case the simulation was made in two steps, one for the TE polarization (*p*-polarized) and one for the TM polarization (*s*-polarized), each one at normal incidence. The two structures were simulated using 6 orders of decomposition for the Rayleigh expansion. It is known that for absorption less materials, few decomposition orders are needed. We also

Optical Materials EXPRESS

performed a convergence study of the structure for the decomposition orders, no changes at 10^{-6} precision for the diffraction efficiency were noticed for more orders than the sixth one.

It was demonstrated by Othera et al. [30] that the conditions of resonant reflection are similar for a planar and a curved substrate once the curvature radius is larger than about 10 grating periods. This condition is satisfied in our case since the tube diameter is 8 mm and the period of the grating is close to 1µm. The simulation was thus performed considering flat substrates in both configurations. The goal of the modeling was to determine the optimized parameters to obtain a resonant reflection in the Near Infra-Red (NIR) region.

2.2. Photosensitive sol-gel formulation and deposition process

A sol-gel procedure previously described was used to obtain a TiO_2-based negative photoresist [28]. A first sol was prepared by reacting titanium tetra iso-propoxide (TIPT from Sigma-Adrich), deionized water, hydrochloric acid (HCl from Roth) and butanol (BuOH from Acros Organics) with a TIPT/H_2O/HCl/BuOH molar composition of 1/0.13/0.82/23.9. A second sol was prepared from TIPT, methanol (MeOH from Sigma-Aldrich) and benzoylacetone (BzAc from Sigma-Aldrich) with a TIPT/MeOH/BzAc molar composition of 1/0.75/20.4 moles. The TiO_2-based photoresist was obtained after mixing the two sols with a BzAc/TIPT molar ratio of 0.6.

The complex TIPT-BzAc makes the solution stable and it provides the photosensitive behavior under UV light where the complex is partially degraded in insoluble species such as carbonates and/or carboxylates. The non-illuminated zones can be removed by washing in ethanol and water while the illuminated zones are insoluble in ethanol. Insolated sol-gel thus acts like a negative photoresist.

For this study, two types of substrates were used: a cylindrical silica substrate (Optics Fichou) with a length of 15 mm, an outer diameter of 10 mm and an inner diameter of 8 mm and a flat silica substrate (1 inch diameter, Neyco NEGS2). Before deposition, each substrate was successively cleaned in three ultrasonic baths of acetone, ethanol and deionized water and then dried under nitrogen.

The sol-gel layer was deposited by dip-coating on the cylindrical substrate or by spin coating on the flat substrate, followed by a thermal treatment at 500°C during 15 minutes to obtain densified layer with high refractive index; this process was repeated three times, the waveguide layer (WL) was obtained by three successive layer depositions to get a thick homogeneous layer without any cracks. The photosensitive layer (PL) was realized using the same sol-gel and deposition conditions, whereas the thermal treatment was done at only 110°C to keep the photosensitive behavior of the layer.

2.3. Planar and cylindrical resonant grating characterization method

The thickness of the waveguide layer was measured by a profilometer Bruker DekTak XT. The refractive index (n) and extinction coefficient (k) were determined on flat substrate using an ellipsometer (UVISEL Horiba Jobin Yvon) associated with Deltapsi2 software. An angle of incidence of 70° and a Tauc-Lorentz model were used. Raman spectroscopy measurements (LabRam ARAMIS) were performed with an excitation wavelength at 633 nm. The profile and depth of gratings were measured by Atomic Force Microscopy (AFM) (Dimension Icon from Bruker) in tapping mode with a tip AppNano ACTA. The Scanning Electron Microscopic (SEM) images were performed using low vacuum mode with NovananoSEM200 (FEI) with HELIX detector.

Measurements of spectral resonances on flat substrates were achieved in reflection with a normal incidence. The source was a white light supercontinuum source (200 nm<λ< 2400 nm), equipped with an infrared linear polarizer (650 nm-2µm) from Thorlabs. A separator blade was used to measure the Transverse Magnetic (TM) and Transverse Electric (TE) mode in reflection.

Optical Materials EXPRESS

The spectra were measured in the near infra-red range with an Ocean Optics NIRQuest spectrometer. Measurements of spectral resonances on the cylinder required a specific setup. This setup was previously described [26]. The characterizations (AFM and SEM) of the cylindrical resonant grating have been performed after a sacrificial operation by breaking the microstructured tube.

3. Results and discussion

3.1. Simulation

The structure modeling with *Chandezon* method was realized to obtain a resonance in reflection around 1500 nm and 1600 nm for TM and TE respectively. For the refractive indexes of the waveguide layer (WL) and the photosensitive layer (PL), ellipsometry measurements were carried out on a planar substrate (Fig. 1). These measurements gave for the considered wavelength (1500 nm), a refractive index of 2.04 (black line) for the waveguide layer and 1.74 for the photosensitive layer (red dotted line) (Fig. 1(a)).

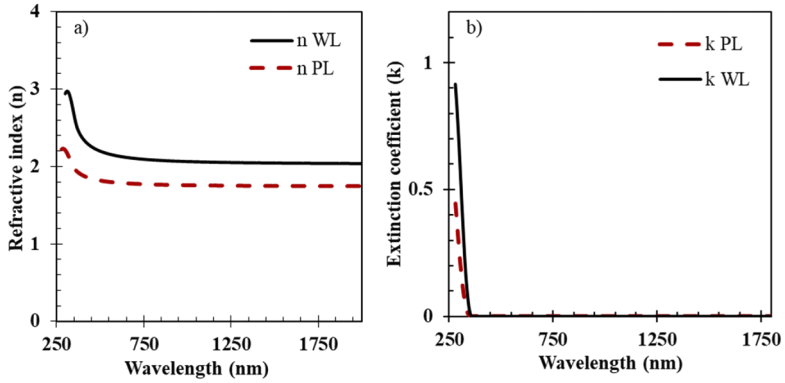

Fig. 1. a) Refractive index and b) extinction coefficient of the waveguide layer (WL) and the photosensitive layer (PL).

The extinction coefficient (k) is zero at 1500 nm for both the waveguide layer and the photosensitive layer as can be seen in Fig. 1(b), which means that there is no absorption at all at this wavelength. Since the waveguide layer has been baked at high temperature, the refractive index is higher. This result is explained by the densification of the sol-gel layer [28].

After simulation, the optimized parameters for the planar WRG are the following: period (Λ) of grating of 1 µm; grating depth (d) of 233 nm, thickness of the photosensitive layer (t) of 280 nm and a waveguide layer thickness (w) of 155 nm (Fig. 2(a)).

By using these parameters, we obtain a spectral resonance for the TM mode at 1506 nm (red dotted line), and at 1582 nm (black dotted line) for the TE mode (Fig. 2(b)). In this article, we consider for all simulated curves the diffraction efficiency, which corresponds to the optical power of a diffracted order compared to the incident power. For resonant reflection, we consider the 0^{th} reflected order.

The shift between the two resonances is attributed to the radiation coefficient (and the effective index of the considered propagative mode) which is different for each polarization.

3.2. Planar resonant grating

In order to realize this demonstrator, a waveguide layer was deposited on a 1 inch silica substrate by spin coating (with a speed at 3000 RPM during 1 min) photo-patternable TiO_2 sol-gel and

Optical Materials EXPRESS

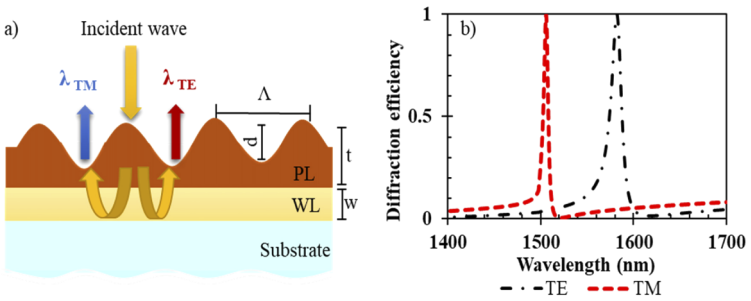

Fig. 2. a) Planar waveguide grating modeling structure and b) its TE and TM resonant reflection under normal incidence.

applying a heat treatment at 500°C. This step was repeated in order to obtain a layer of 155 nm, using two successive layer depositions. The thickness was measured by a profilometer.

For both configurations (planar and cylindrical WRG), the deposition of layer was performed in clean room environment, to guarantee temperature and humidity control (25°C and 50% respectively). The sol-gel solution was filtered thanks to a syringe with an Acrodisc syringe filter (from Sigma-Aldrich), composed of a PVDF membrane with pores of 200 nm diameter. The obtained waveguide layer was transparent and it did not show any cracks. The Raman spectrum of the waveguide layer (black line) showed some characteristic peaks of a crystalline structure at 144 cm^{-1}, 197 cm^{-1}, 399 cm^{-1}, 515 cm^{-1} and 639 cm^{-1}. These peaks correspond to the anatase phase [31] of the TiO_2 material (Fig. 3).

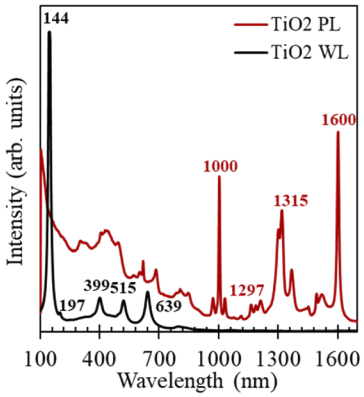

Fig. 3. Raman spectra of TiO_2 waveguide later (WL) and TiO_2 photosensitive layer (PL).

In a second technological step, a photosensitive layer is deposited on top of the waveguide layer by spin coating, using the same photo-patternable TiO_2 sol-gel. A thermal treatment at lower temperature (110°C during 90 minutes) was made to evaporate the solvents, while keeping the photosensitive behavior of the TiO_2 sol-gel. Indeed, the Raman spectrum (Fig. 3 red line) showed multiple peaks but no features of the crystallized TiO_2 phase. In accordance with Oda et al. [31], the peaks at 1600 and 1000 cm^{-1} were assigned to 8b and 12 vibration modes of the Phenyl group of BzAc, the peaks at 1297 and 1315 cm^{-1} could be attributed to the symmetric vibration of the C = C=C bond of BzAc molecules that chelate the titanium atoms [32]. It is clear from these results that the TiO_2 layer is not pure and still contains organic functions, but in order to simplify the reading, we will keep in the rest of the manuscript the name TiO_2 for xerogel comprising organic functions.

Optical Materials EXPRESS

The thickness of the obtained photosensitive layer was measured by the profilometer to be 280 nm. The refractive indexes obtained by ellipsometry measurements are the same as in Fig. 1 (red dotted line).

The fabrication of the grating was performed in three steps as illustrated in Fig. 4. First, a chromium phase mask with a grating of 1µm period was placed above the photosensitive layer (Fig. 4(a)). Then, a hard contact was created between the substrate and the chromium mask using vacuum, followed by UV illumination at 365 nm wavelength during 10 minutes in order to degrade the BzAc/TIPT complex and to make the illuminated areas not soluble in ethanol as shown in Fig. 4(b). In the final step, the samples were rinsed in ethanol and water during 60 seconds to remove the unexposed areas as illustrated in Fig. 4(c).

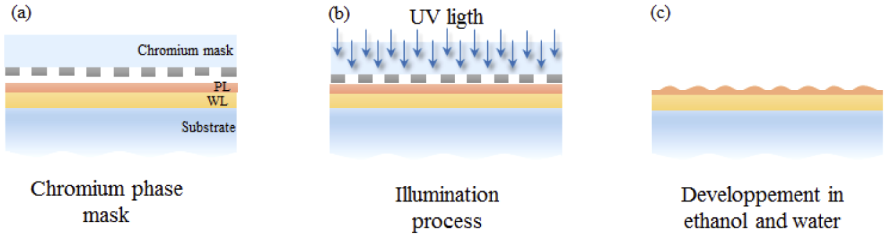

Fig. 4. UV illumination process for the grating writing a) chromium phase mask b) illumination process with UV light c) development of grating in ethanol and water.

The grating was printed on a 5×2 mm^2 area (size of the 1 µm period grating). The optical image (Fig. 5(a)) shows the diffraction of visible light by the grating, which indicates the localization of the microstructured area. SEM images of the top view of the sample (Fig. 5(b)) show a periodic grating with a period of 1µm. These results are corroborated by AFM measurements (Fig. 5(c)). The depth of the grating (d) was estimated to be 230 nm and the period (Λ) 1µm.

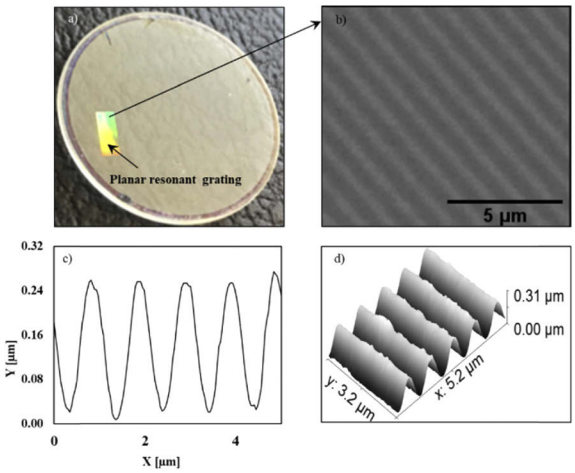

Fig. 5. Planar TiO_2 grating characterization a) picture of the sample b) SEM of the top view of grating c) AFM grating profile and d) AFM 3D topography grating.

No further processes have been carried out to reduce roughness, for example plasma or heat treatment based post-process. Thanks to the direct UV writing process of the sol-gel layer, grating roughness is limited compared to etching process and is mainly caused by the roughness of the sol-gel layer deposition which is much below 10 nm.

Optical Materials EXPRESS

Subsequently, the sample was measured in reflection in normal incidence for both polarizations. The spectra (Fig. 6(a)) showed two experimental resonances in the NIR at 1506 nm (gray line) and 1582 nm (blue line) for the TM and TE mode, respectively. These results indicate a very good agreement between the experimental setup and the simulation. The resonance reflection efficiency for the experimental resonances was lower than theoretically expected, the experimental TE peak was measured at 11% reflectance and the experimental TM peak had only 7% reflectance. The comparison of simulated and normalized experimental results (Fig. 6(b)) shows that the positions of the peaks correspond very well. However, their width are quite different. Comparing the FWHM values of the normalized experimental and simulated peaks, we find for the TM mode 26 nm and 5 nm, respectively, while the corresponding values for the TE mode are 29 nm and 14 nm. This important difference is mainly explained by the roughness of the grating, which leads to diffusion losses, and the inhomogeneity of the grating due to the chromium mask transfer under hard contact. Both effects spectrally enlarge the reflection peak and decrease the peak reflection efficiency. The experimental values would notably improve with better chromium mask transfer or using a direct LIL process for the grating printing. Nevertheless, the results show the possibility of making resonant gratings with only one photo-patternable sol-gel, which to our knowledge is completely original and unique.

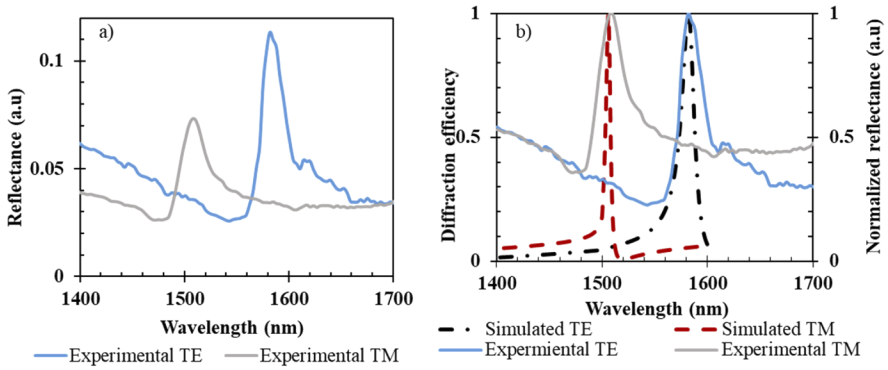

Fig. 6. a) Experimental resonance spectra and b) comparison between experimental and simulated normalized resonances.

3.3. *Cylindrical resonant grating*

In this part, the goal is to obtain a resonant grating inside a cylindrical substrate, which closes perfectly on itself, that is, without any stitching errors. This is possible since the grating is printed using the projection of a periodic pattern created from a perfect phase mask with an integer number of grating periods. First, the waveguide and the photosensitive layer were fabricated using the same number of layers and thermal treatments as in the planar case. To deposit the sol gel layer on the inner wall of a cylindrical substrate (tube), a dip-coating technique was the only possibility. First, the waveguide layer was deposited by 3 successive layer depositions using the dip coating process. This process was performed by the immersion of the tube into a small appropriate tank containing the sol-gel solution and its withdrawal at constant speed of 7 cm/min. After the removal of the tube from the solution, a homogeneous liquid film was formed on both tube's surfaces (outer and inner of the tube). Thickness homogeneity of the layers was ensured by a well control of the dip coating parameters during the withdrawal of the tube, thanks to an anti-vibrations table and a constant speed. Each layer deposition was followed by a 15 min baking at 500 °C. In order to have an idea of the thickness of the waveguide layer, the same process was performed on a flat silica substrate. Studies on sacrificial tubes that were broken to be able to measure the layer height indicate a similar thickness between the waveguide inside the cylinder

Optical Materials EXPRESS

and the one on the flat substrate produced under the same conditions [26]. For this sample, the thickness of the waveguide layer was estimated to be around 155 nm. The TiO_2 is in its anatase phase with a refractive index of 2.04 at 1500 nm wavelength.

After that, a photosensitive layer was deposited by dip coating, also at 7 cm/mn, followed by a low temperature thermal treatment. The thickness was measured at 250 nm.

The grating was printed on the inner wall of the cylinder using a phase mask, as described in Ref. [24]. The phase mask is a radial diffraction grating designed to maximize the efficiency of the 1^{st} transmitted orders over the entire range of the radial corrugation, while the 0^{th} transmitted order propagates parallel to the tube axis and does not interfere with the 1^{st} orders at the cylinder wall. The 2^{nd} diffraction orders are evanescent. The grating has a constant angular period ($\Lambda_{\varphi-pm)}$ of 480 µrad which creates a variable spatial period according to the radial position r ($R_i < r < R_e$), with R_i and R_e the internal and external radius respectively. Assuming an inner tube radius of r = 4 mm, the final grating period at the inner wall will have a spatial period of $\Lambda = R \cdot (\Lambda / 2) = 960$ nm. The details on the phase mask design and the fabrication are given in Ref. [24]. The phase mask is illuminated under normal incidence with a circular polarization by a 100 mW laser at wavelength 355 nm [25].

The photosensitive layer on the cylindrical substrate was illuminated during 10 minutes. The sample was developed in ethanol and rinsed in water during 60 seconds.

After this process, the grating inside the cylinder was visible by the diffraction of white light (Fig. 7(a)). The depth of the grating was estimated at 185 nm and the period at 960 nm. The grating profile (Fig. 7(b), (c) and (d)) was analyzed using AFM and SEM analysis on a broken piece.

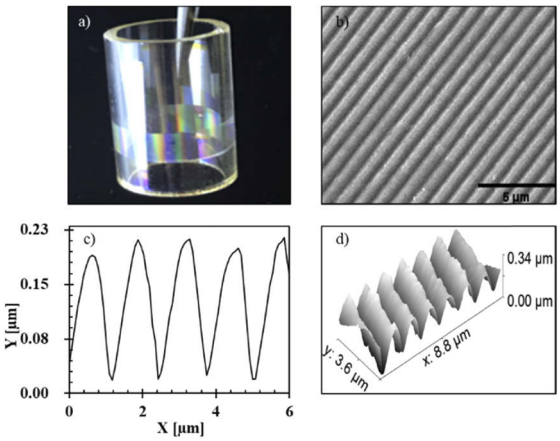

Fig. 7. Characterization of a TiO_2 grating a) on a cylinder photo of the sample b) SEM top view of cylindrical grating c) AFM profile measurement d) AFM grating topography.

The resonance characterization of the cylindrical device used a special optical set-up as described in Ref. [25]. In order to have a complete and homogeneous illumination of the grating, a cylindrical, circularly polarized wave whose center coincides with the cylinder axis is necessary.

The circular polarization was obtained by a linear polarizer and a quarter wave plate. The beam was then reflected by a metallized cone situated on the axis of the tube, creating a homogeneous illumination of the inner tube wall in a holistic manner. With the circular polarization, TE and TM waveguide modes are excited everywhere and subsequently back-reflected in the incident direction. The reflective cone enables this reflected wave to be detected and measured after being separated from the incoming beam by a beam splitter. The reflected beam is then analyzed by the spectrophotometer in order to measure the efficiency (Fig. 8).

Optical Materials EXPRESS

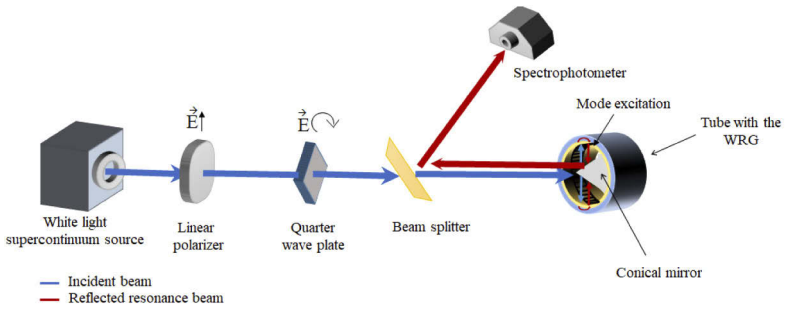

Fig. 8. Cylindrical resonance set-up.

The recorded spectrum shows two peaks, one at 1445 nm for the TM mode and one at 1507 nm for the TE mode as illustrated in Fig. 9(a).

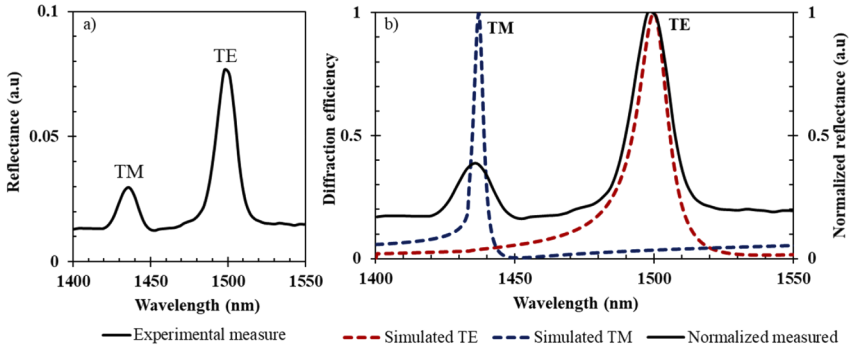

Fig. 9. a) Experimental resonance measured on the cylindrical resonant grating b) superposition of simulated TE (red dotted line) and TM (blue dotted line) resonance spectra with the normalized experimental measure in the cylindrical resonant grating (black line).

Figure 9(b) exhibits the experimental normalized reflected resonance (black line) for TE and TM compared with the simulated curves (dotted lines). Only relative efficiencies have been measured due to the difficulty of measuring an accurate reference for the reflectance spectrum. The theoretical resonances are situated at 1499 nm for TE (red dotted line) and 1437 nm for TM (blue dotted line). The experimental spectrum reveals that the TE and TM resonances occur at the same time since both modes (TE and TM) are excited during the illumination.

The reflectance for the TM mode was lower than the TE mode. This difference is probably explained by the separator blade which is composed of multiple layers that generate a decrease in reflectance for the TM mode when placed at 45° incidence angle. The simulated and experimental normalized spectra of the cylindrical resonant grating show a good agreement, with a deviation in the spectral position of the peaks of about 8 nm for both TM and TE. The measured TE and TM peaks are separated by 70 nm as is expected by the theory.

The FWHM values obtained for the normalized experimental and simulated reflection peaks were 20 nm and 14 nm, respectively, in the TE case and 22 nm and 5 nm, respectively, in the TM case. The difference may be due to imperfections of grating but the circular or infinity grating inside the cylindrical substrate generates narrower resonance peaks which seems to be confirmed in the present case.

Optical Materials EXPRESS

4. Conclusion

The present paper has demonstrated the experimental phenomenon of resonant reflection in a planar and cylindrical resonant grating made with sol-gel. The sol-gel allowed to obtain a waveguide layer with a high refractive index using a thermal treatment at high temperature. Thanks to the photosensitive property of sol-gel at low temperature heat treatment, it was possible to print a grating using a simple photolithography method without any etching process, in the case of a planar as well as a cylindrical substrate. The purpose of this paper was to demonstrate the existence of a resonance in the near infrared for both types of substrates, and to compare it with theoretical simulation results. We found a good agreement for the spectral position of the simulated and experimental resonances for TE and TM polarization. However, experimental efficiencies are much below the expected theoretical ones. This can be explained by the inhomogeneity of the grating (grating profile, grating depth, line space ratio of the grating period) as well as grating surface roughness. Moreover, resonant reflection measurements still remain a challenge for measuring resonant reflection inside a tube with high accuracy. The authors are currently working on a monolithic sensor approach with the cone fabricated directly inside the tube, avoiding the complex alignment procedure. By this way, the authors plan to develop a new generation of monolithic and miniaturized sensors for bio or gas detection.

Finally, the complete sol-gel approach for fabricating RWG is a very promising technological approach since it enables lossless propagation of grating modes and, at the same time, is compatible to lithographic grating printing because of its photosensitivity. Due to its well-known mechanical and chemical stability, as well as its functional (optical) properties, the sol-gel approach can be considered as a unique approach for the fabrication of RWG on non-planar substrates, such as cylindrical based shapes or curved substrates.

Funding

Région Auvergne-Rhône-Alpes (Pack Ambition Recherche 2018, MICROSOLEN project); Université de Lyon (Scientific Breakthrough Program, IPPON Project); Centre National de la Recherche Scientifique CNRS (French RENATECH+, NanoSaintEtienne).

Disclosures

The authors declare no conflicts of interest.

References

1. M. Neviere, R. Petit, and M. Cadilhac, "About the theory of optical grating coupler-waveguide systems," Opt. Commun. **8**(2), 113–117 (1973).
2. L. Mashev and E. Popov, "Zero order anomaly of dielectric coated gratings," Opt. Commun. **55**(6), 377–380 (1985).
3. G. Quaranta, G. Basset, O. J. F. Martin, and B. Gallinet, "Recent advances in resonant waveguide gratings," Laser Photonics Rev. **12**(9), 1800017 (2018).
4. M. G. Moharam and T. K. Gaylord, "Rigorous coupled-wave analysis of planar-grating diffraction," J. Opt. Soc. Am. **71**(7), 811–818 (1981).
5. J. Chandezon, G. Raoult, and D. Maystre, "A new theoretical method for diffraction gratings and its numerical application," J. Opt. **11**(4), 235–241 (1980).
6. G. Quaranta, G. Basset, O. J. F. Martin, and B. Gallinet, "Color-selective and versatile light steering with up-scalable subwavelength planar optics," ACS Photonics **4**(5), 1060–1066 (2017).
7. S. Isaacs, A. Hajoj, M. Abutoama, A. Kozlovsky, E. Golan, and I. Abdulhalim, "Resonant grating without a planar waveguide layer as a refractive index sensor," Sensors **19**(13), 3003 (2019).
8. F.-J. Haug, K. Söderström, A. Naqavi, and C. Ballif, "Excitation of guided-mode resonances in thin film silicon solar cells," Mater. Res. Soc. Symp. Proc. **1321**, mrss11-1321-a17-12 (2011).
9. J. Barbé, A. F. Thomson, E.-C. Wang, K. McIntosh, and K. Catchpole, "Nanoimprinted TiO_2 sol-gel passivating diffraction gratings for solar cell applications," Prog. Photovoltaics **20**(2), 143–148 (2012).
10. P. Reader-Harris, A. Ricciardi, T. Krauss, and A. Di Falco, "Optical guided mode resonance filter on a flexible substrate," Opt. Express **21**(1), 1002 (2013).

Optical Materials EXPRESS

11. A. S. P. Chang, K. J. Morton, H. Tan, P. F. Murphy, W. Wu, and S. Y. Chou, "Tunable liquid crystal-resonant grating filter fabricated by nanoimprint lithography," IEEE Photonics Technol. Lett. **19**(19), 1457–1459 (2007).
12. J. M. Ziebarth, A. K. Saafir, S. Fan, and M. D. McGehee, "Extracting light from polymer light-emitting diodes using stamped Bragg gratings," Adv. Funct. Mater. **14**(5), 451–456 (2004).
13. T. J. Trout, J. J. Schmieg, W. J. Gambogi, and A. M. Weber, "Optical photopolymers: design and applications," Adv. Mater. **10**(15), 1219–1224 (1998).
14. K. J. Lee, R. LaComb, B. Britton, M. Shokooh-Saremi, H. Silva, E. Donkor, Y. Ding, and R. Magnusson, "Silicon-layer guided-mode resonance polarizer with 40-nm bandwidth," IEEE Photonics Technol. Lett. **20**(22), 1857–1859 (2008).
15. D. Rosenblatt, A. Sharon, and A. A. Friesem, "Resonant grating waveguide structures," IEEE J. Quantum Electron. **33**(11), 2038–2059 (1997).
16. K. Bougot-Robin, J.-L. Reverchon, M. Fromant, L. Mugherli, P. Plateau, and H. Benisty, "2D label-free imaging of resonant grating biochips in ultraviolet," Opt. Express **18**(11), 11472–11482 (2010).
17. C.-L. Jia, K.-M. Wang, X.-L. Wang, X.-J. Zhang, and F. Lu, "Formation of c-axis oriented ZnO optical waveguides by radio-frequency magnetron sputtering," Opt. Express **13**(13), 5093–5099 (2005).
18. K.-S. Kim and S. E. Pratsinis, "Manufacture of optical waveguide preforms by modified chemical vapor deposition," AIChE J. **34**(6), 912–921 (1988).
19. R. Asquini, A. Buzzin, D. Caputo, and G. de Cesare, "Integrated evanescent waveguide detector for optical sensing," IEEE Trans. Compon., Packag., Manuf. Technol. **8**(7), 1180–1186 (2018).
20. Q. Xie, M. H. Hong, H. L. Tan, G. X. Chen, L. P. Shi, and T. C. Chong, "Fabrication of nanostructures with laser interference lithography," J. Alloys Compd. **449**(1-2), 261–264 (2008).
21. C. Lu and R. H. Lipson, "Interference lithography: a powerful tool for fabricating periodic structures," Laser Photonics Rev. **4**(4), 568–580 (2010).
22. Y. Huang, L. Liu, M. Johnson, A. C. Hillier, and M. Lu, "One-step sol-gel imprint lithography for guided-mode resonance structures," Nanotechnology **27**(9), 095302 (2016).
23. H. Hirshy, S. G. Scholz, Y. Jourlin, S. Tonchev, S. Reynaud, A. Boukenter, and O. Parriaux, "2N Period submicron grating at the inner wall of a metal cylinder," Microsyst. Technol. **20**(10-11), 1833–1837 (2014).
24. L. Berthod, M. Bichotte, I. Verrier, C. Veillas, T. Kämpfe, F. Vocanson, M. Langlet, J. Laukkanen, O. Parriaux, and Y. Jourlin, "Efficient reversible phase mask for TiO_2 submicron gratings directly printed on cylindrical surfaces," Opt. Express **25**(8), 9003–9009 (2017).
25. E. Koussi, H. Bruhier, M. A. Usuga Higuita, I. Verrier, C. Veillas, T. Kämpfe, S. Reynaud, N. Crespo-Monteiro, O. Parriaux, and Y. Jourlin, "Resonant reflection from cylindrical grating-waveguide under holistic excitation," IEEE Photonics J. **12**(2), 1–11 (2020).
26. L. Berthod, O. Shavdina, F. Vocanson, M. Langlet, O. Dellea, C. Veillas, S. Reynaud, I. Verrier, and Y. Jourlin, "Colloidal photolithography applied to functional microstructure on cylinder based on photopatternable TiO_2 sol-gel," Microelectron. Eng. **177**, 46–51 (2017).
27. F. Tricot, F. Vocanson, D. Chaussy, D. Beneventi, S. Reynaud, Y. Lefkir, and N. Destouches, "Photochromic Ag:TiO_2 thin films on PET substrate," RSC Adv. **4**(106), 61305–61312 (2014).
28. S. Briche, Z. Tebby, D. Riassetto, M. Messaoud, E. Gamet, E. Pernot, H. Roussel, O. Dellea, Y. Jourlin, and M. Langlet, "New insights in photo-patterned sol-gel-derived TiO_2 films," J. Mater. Sci. **46**(5), 1474–1486 (2011).
29. L. Berthod, O. Shavdina, I. Verrier, T. Kämpfe, O. Dellea, F. Vocanson, M. Bichotte, D. Jamon, and Y. Jourlin, "Periodic TiO_2 nanostructures with improved aspect and line/space ratio realized by colloidal photolithography technique," Nanomaterials **7**(10), 316 (2017).
30. Y. Ohtera, S. Iijima, and H. Yamada, "Guided-mode resonance in curved grating structures," Opt. Lett. **36**(9), 1689–1691 (2011).
31. S. Oda, H. Uchiyama, and H. Kozuka, "Thermoplasticity of sol-gel-derived titanoxanes chemically modified with benzoylacetone," J. Sol-Gel Sci. Technol. **70**(3), 441–450 (2014).
32. H. Tang, K. Prasad, R. Sanjinès, P. E. Schmid, and F. Lévy, "Electrical and optical properties of TiO_2 anatase thin films," J. Appl. Phys. **75**(4), 2042–2047 (1994).